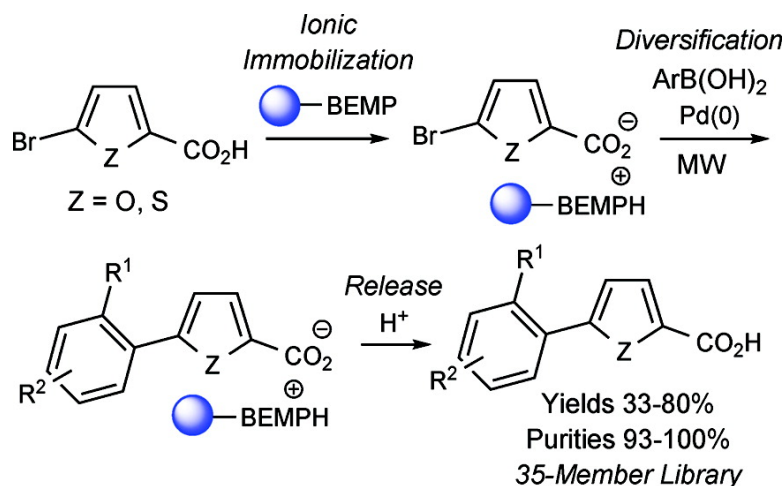


Ionic Immobilization, Diversification, and Release: Application to the Generation of a Library of Methionine Aminopeptidase Inhibitors

Punitha Vedantham, Jennifer M. Guerra, Frank Schoenen, Min Huang, Parul J. Gor, Gunda I. Georg, Jenna L. Wang, Benjamin Neuenswander, Gerald H. Lushington, Lester A. Mitscher, Qi-Zhuang Ye, and Paul R. Hanson

J. Comb. Chem., 2008, 10 (2), 185-194 • DOI: 10.1021/cc700085c • Publication Date (Web): 29 December 2007

Downloaded from <http://pubs.acs.org> on March 25, 2009



More About This Article

Additional resources and features associated with this article are available within the HTML version:

- Supporting Information
- Access to high resolution figures
- Links to articles and content related to this article
- Copyright permission to reproduce figures and/or text from this article

[View the Full Text HTML](#)



ACS Publications
 High quality. High impact.

Ionic Immobilization, Diversification, and Release: Application to the Generation of a Library of Methionine Aminopeptidase Inhibitors

Punitha Vedantham,[†] Jennifer M. Guerra,[†] Frank Schoenen,[‡] Min Huang,^{||}
Parul J. Gor,[†] Gunda I. Georg,^{§,±} Jenna L. Wang,[†] Benjamin Neuenswander,[‡]
Gerald H. Lushington,[†] Lester A. Mitscher,[§] Qi-Zhuang Ye,^{||,⊥} and Paul R. Hanson^{*,†}

Department of Chemistry, University of Kansas, 1251 Wescoe Hall Drive, Lawrence, Kansas 66045, the KU Chemical Methodologies and Library Development Center of Excellence, 1501 Wakarusa Drive, Lawrence, Kansas 66047, Department of Medicinal Chemistry, Center for Cancer Experimental Therapeutics and Drug Discovery Program, Higuchi Biosciences Center, University of Kansas, 1251 Wescoe Hall Drive, Lawrence, Kansas 66045, and The High Throughput Screening Laboratory, University of Kansas, 1501 Wakarusa Drive, Lawrence, Kansas 66047

Received May 24, 2007

Development of an ionic immobilization, diversification, and release method for the generation of methionine aminopeptidase inhibitors is reported. This method involves the immobilization of 5-bromofuran-2-carboxylic acid and 5-bromothiophene-2-carboxylic acid onto PS-BEMP, followed by Suzuki reaction on a resin-bound intermediate and subsequent release to provide products in moderate yields and excellent purities. Compound potencies were evaluated on the Co(II), Mn(II), Ni(II), and Fe(II) forms of *Escherichia coli* MetAP1. The furoic-acid analogs were found to be Mn(II) selective with IC₅₀ values in the low micromolar range. Qualitative SAR analysis, supplemented by molecular modeling studies, provides valuable information on structural elements responsible for potency and selectivity.

Introduction

Methionine aminopeptidase (MetAP) is a metalloenzyme responsible for the removal of a methionine residue from the N-terminus of nascent proteins, which is an important cotranslational modification.¹ In eukaryotes, two isozymes (type I and type II MetAPs) catalyze the removal with similar substrate specificities.² Fumagillin, ovalicin, and TNP-470 are naturally occurring compounds that possess antiangiogenic properties and selectively inhibit human type II MetAP.³ The bengamides are a family of compounds that inhibit the growth of cancer cells and inhibit the two isozymes nonselectively.⁴ This suggests that human MetAPs are possible molecular targets of these anticancer agents. In contrast, prokaryotes possess only one MetAP, either type I (eubacteria) or type II (archaea), and deletion of the single enzyme was demonstrated to be lethal in *Escherichia coli*⁵ and *Salmonella typhimurium*.⁶ The essential function of this enzyme in bacteria suggests that it is a promising target for developing antibacterial therapeutics, broad-spectrum antibiotics, and antifungal drugs.⁷

All MetAPs require a divalent metal ion such as Mn(II), Fe(II), Co(II), Ni(II), or Zn(II) for activity. However, the relative importance of each metal in vivo remains uncertain. One primary challenge in the development of MetAP inhibitors as antibacterial and anticancer agents is the definition of the participant metal ions used by MetAP in vivo and the discovery of MetAP inhibitors that inhibit corresponding metalloforms in vivo. The generation of new metalloform-selective MetAP inhibitors is valuable for identification of active pharmacophores and for the subsequent definition of which metals are physiologically important for MetAP activation.

Combinatorial chemistry coupled with high-throughput screening (HTS) has dramatically increased the number of compounds that are screened against a variety of biological targets. In this regard, solid-phase organic synthesis (SPOC) has gained much interest because it offers several advantages, including simplified workup procedures, avoiding time-consuming intermediate purification procedures, and automation to facilitate the production of a large number of compounds in a relatively short period of time. This is particularly useful when the overall aim is the generation of high-quality lead structures that serve as optimum starting points for further development.⁸ Despite these features, issues related to scale-up and validation-time warrant continuous development of new methods. In the present study, we describe our efforts toward the design and library-generation of methionine aminopeptidase inhibitors using a new method involving attachment of substrate to a resin via an ionic bond, thus avoiding a linker. The method involves a three-step

* To whom correspondence should be addressed. E-mail: phanson@ku.edu. Phone: (785) 864-3094. Fax: (785) 864-5396.

[†] Department of Chemistry.

[‡] KU Chemical Methodologies and Library Development Center of Excellence.

[§] Department of Medicinal Chemistry.

^{||} The High Throughput Screening Laboratory.

[⊥] Current Address: Department of Biochemistry and Molecular Biology, Indiana University School of Medicine, 635 Barnhill Drive, MS4053, Indianapolis, IN 46202.

[±] Department of Medicinal Chemistry, University of Minnesota, 717 Delaware St SE, Room 452, Minneapolis, MN 55455.

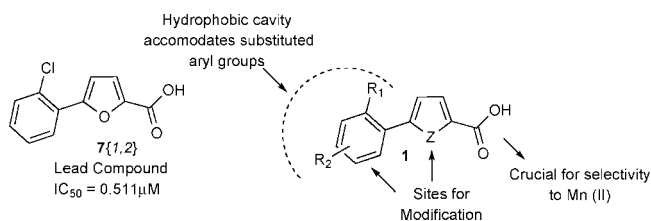


Figure 1. Key elements in library design.

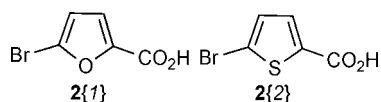


Figure 2. Core heterocyclic acids used for library production.

sequence termed “ionic immobilization, diversification, and release”, where a basic resin is used to immobilize an acid, which is subjected to Suzuki reaction, followed by acid-assisted cleavage, ultimately providing products with no additional functionality, and leaving no trace of solid-phase synthesis. The ionic attachment plays the role of a “traceless linker”, wherein an ionic bond replaces the resin attachment between the substrate and the resin. Moreover, because the acid group is an essential pharmacophore for inhibition of methionine aminopeptidase, this new method precisely delivers requisite biaryl acids without the additional use of protecting groups or masking agents. As a final note, biological evaluation, supplemented by molecular modeling, reveals structural elements that contribute to inhibitory potency and selectivity against the different metalloforms tested.

Library Design

Initially, high-throughput screening led to the discovery of several nonpeptidic inhibitors that are potent and metal selective, with 7{1,2} emerging as the lead compound for study (Figure 1).⁹ A series of analogs of 5-phenylfuran-2-carboxylic acid were prepared and evaluated on Co(II), Mn(II), Ni(II), and Fe(II) forms of *E. coli* MetAP.¹⁰ Substitution of the free carboxyl group by various amide and sulfonamide,¹¹ ester, hydrazide, cyanomethyl and hydroxymethyl groups resulted in reduction of potency.¹⁰ While the hydroxamate was as potent as 7{1,2}, it was nonselective against the four metalloforms tested. Substitution at the 2-position on the phenyl ring resulted in a noncoplanar conformation of the two aromatic rings, which was found to be essential for potency. These studies confirmed two key structural features essential for activity, namely, the carboxyl group, which provides the main docking interaction with the Mn(II) ions, and a noncoplanar conformation of the two aromatic rings.

Under this premise, we designed a small library of compounds, which share substructural diversity at the central core ring and the aromatic ring. Design elements included replacing the central furan ring with thiophene ring, varying the nature/type of substituents on the phenyl ring, sequentially changing the position of the substituents on the aromatic ring (such as 2,3-, 2,4-, and 2,5-), and replacing the phenyl ring by different aromatic groups such as naphthyl, biphenyl, thiophenyl, and indolyl. Figures 2 and 3 represent the

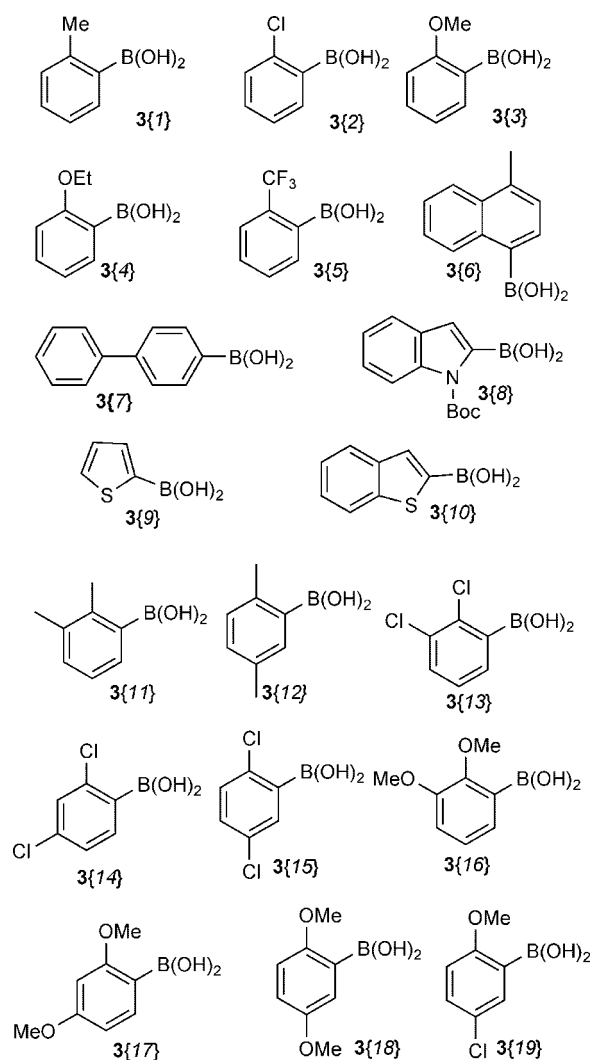


Figure 3. Mono- and disubstituted arylboronic acids used for library production.

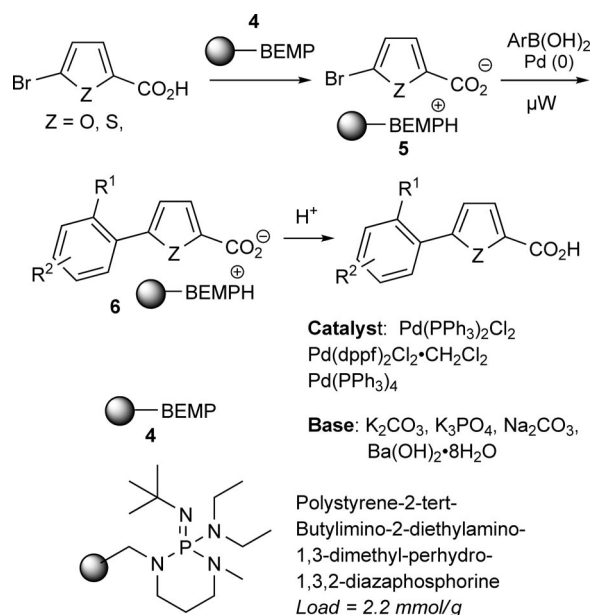
different core acids and arylboronic acids that were used in the library, respectively.

Results and Discussion

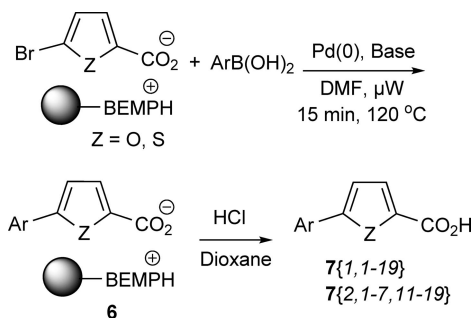
Classical synthesis of biaryl acids of type 1 involves Suzuki coupling of heterocyclic acids 2{1,2} with commercially available arylboronic acids. In an attempt to avoid tedious aqueous work up, acid–base extractions, or protecting groups/masking agents, an alternative method amendable to high-throughput synthesis using sequestering reagents was envisioned. A variety of basic resins including PS-TBD, PS-trisamine, Amberlyst NH₄OH, and PS-BEMP have been known to sequester acidic species as the corresponding ion pair. Among these PS-BEMP is proven to be a general sequestering agent for a broad range of scaffolds including purines,¹² sulfonamides,¹³ thiobenzylimidazoles,¹⁴ and trichloroacetyl carbamates.¹⁵ Its generality, superiority over other resins, low nucleophilicity, high basicity, and better dispersion in polar solvents¹⁶ encouraged us to use this as an immobilization reagent. Presented below are the details pertaining to the library optimization and generation.

In the immobilization step, the acid was loaded on resin 4 by shaking of the reaction mixture in DMF/DMSO

Scheme 1. Chromatography-Free Synthesis of Biaryl Acids



Scheme 2. General Protocol for Library Production



overnight, followed by filtration and sequential resin washes with MeOH/CH₂Cl₂, to provide intermediate **5** (Scheme 1). To quantitatively determine the amount of acid loaded, a sample of the ion-pair **5** (40 mg) was treated with HCl (4 N) in dichloromethane at room temperature to yield 9 mg of the acid, which corresponds to 56% loading of the resin. To increase the amount of material obtained after the “immobilization–cleavage” sequence, different variations of the loading step and the cleavage step were explored; however, none of these variations resulted in significantly higher yields.¹⁷ Nonetheless, to investigate the feasibility of our method, intermediate **5** was subjected to Suzuki reaction with **3{1}**, which upon subsequent cleavage with 4 N HCl in dioxane¹⁸ and filtration through a SiO₂ SPE cartridge, yielded product **7{1,1}** in moderate yield (over two steps) and excellent purity (¹H NMR and LC-MS). Encouraged by this result, the generality and scope of this method using a variety of arylboronic acids was investigated. Initial experiments were carried out to optimize catalyst, base, time, and temperature. The optimal conditions were found to be microwave irradiation for 15 min at 120 °C using Pd(PPh₃)₂Cl₂ and K₂CO₃ for all substrates except **3{5,8–11}**, for which Pd(PPh₃)₄/K₃PO₄ proved to be a suitable system.

A representative library with different arylboronic acids in a parallel format was generated as follows. The loading, cleavage, and resin-wash sequences were carried out on Bodhan MiniBlock SPE stations. Suzuki reactions were

Table 1. Representative Examples of Library Members

entry	library member	yield (%) ^a	purity (%) ^b
1	7{1,1}	46	94
2	7{1,2}	48	93
3	7{1,3}	51	95
4	7{1,4}	36	98
5	7{1,7}	48	97
6	7{1,12}	50	100
7	7{1,13}	36	100
8	7{1,15}	80	93
9	7{1,16}	43	100
10	7{1,18}	35	100
11	7{1,19}	50	100
12	7{2,1}	51	100
13	7{2,2}	50	97
14	7{2,3}	40	100
15	7{2,4}	42	100
16	7{2,12}	33	96
17	7{2,14}	80	100

^a Yields are calculated over 2 steps. ^b Purities are determined by RP HPLC-MS-UV.

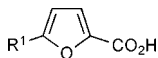
carried out in an automated Emrys Optimizer single-mode microwave reactor. The solvent was evaporated in a GeneVac EZ-2 Plus parallel evaporator, and the crude material was analyzed by RP HPLC-MS-UV at 215 nm. The overall yields (over two steps) were 33–80%, and the purities were 93–100% (Table 1).¹⁹

The potency of compounds **7{1,2–19}** and **7{2,1–7,11–15,17–19}** were tested against recombinant *E. coli* MetAP1, which was purified as an apoenzyme as reported previously.²⁰ The inhibitory activity of these compounds on the four metalloforms of *Ec*MetAP1 is summarized in Tables 2 and 3.

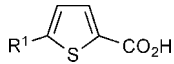
The kinetics measurements reported in Tables 2 and 3 suggest substantial affinity variation as a function of phenyl and other aromatic substitutions on the furan and thiophene rings. The combination of such kinetics data with ligand–receptor information (as can be derived from *in silico* docking analysis relative to the available MetAP crystal structures) affords one with the potentially powerful analytical tool of systematic and information-rich receptor-based quantitative structure–activity relationship analysis. This goal forms the basis for the subsequent section.

Computational Methods

The full set of 33 furan- and thiophene-carboxylic acid inhibitors were drawn in SYBYL²¹ in both neutral and carboxylate form. The compounds were structurally optimized using the Tripos force field²² and Gasteiger–Marsili²³ charges (default SYBYL molecular mechanics minimization convergence settings). A model of the MetAP receptor was prepared from the 1XNZ crystal structure (*E. coli* methionine aminopeptidase inhibited by **7{1,2}**)⁹ by removing the cocrystallized ligand and crystallographic waters and adding Gasteiger–Marsili charges to the remaining structure (*in situ* manganese ions were presumed to be dicationic). The ligands were then docked into the receptor using AutoDock²⁴ requesting 50 poses per ligand as evaluated using the standard genetic algorithm’s search algorithm. For both the neutral and carboxylate ligand manifolds, we attempted to train receptor-based quantitative structure–activity relationship models to the observed affinity data for ligand complexation

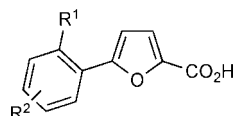
Table 2. Inhibition of *EcMetAP1* by Aryl Furan and Thiophene Carboxylic Acid


entry	library member	R ¹	IC ₅₀ (μM)			
			Mn(II)	Co(II)	Fe(II)	Ni(II)
1	7{1,2}	2-chlorophenyl	0.511 ^a	138.298 ^a	141.0 ^a	116.4 ^a
2	7{1,3}	2-methoxyphenyl	0.55 ^a	131.98 ^a	200 ^a	200 ^a
3	7{1,4}	2-ethoxyphenyl	0.48	41.90	50.0	50.0
4	7{1,5}	2-trifluoromethylphenyl	0.15	50.00	31.4	50.0
5	7{1,6}	4-methylnaphthyl	0.67	50.00	50.0	50.0
6	7{1,7}	biphenyl	0.77	30.2	50.0	37.7
7	7{1,8}	1 <i>H</i> -indolyl	0.46	50.00	50.0	45.8
8	7{1,9}	thiophenyl	1.28	50.0	50.0	50.0
9	7{1,10}	benzothiophenyl	2.75	50.00	41.6	32.2

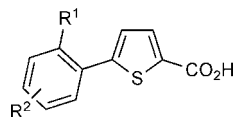


entry	library member	R ¹	IC ₅₀ (μM)			
			Mn(II)	Co(II)	Fe(II)	Ni(II)
10	7{2,1}	2-methylphenyl	1.51	35.8	50.0	50.0
11	7{2,2}	2-chlorophenyl	3.5	45.3	50.0	50.0
12	7{2,3}	2-methoxyphenyl	4.99	27.3	47.7	45.7
13	7{2,4}	2-ethoxyphenyl	5.08	50.00	50.0	50.0
14	7{2,5}	2-trifluoromethylphenyl	0.89	50.00	50.0	50.0
15	7{2,6}	4-methylnaphthyl	17.89	50.0	50.0	50.0
16	7{2,7}	biphenyl	3.58	49.2	50.0	28.7

^a The potencies of these compounds have been published earlier.

Table 3. Inhibition of *EcMetAP1* by Compounds with Disubstitution on Phenyl Ring of Furan and Thiophene Carboxylic Acid


entry	library member	R ¹	R ²	IC ₅₀ (μM)			
				Mn(II)	Co(II)	Fe(II)	Ni(II)
17	7{1,11}	Me	3-Me	0.53	50.00	26.4	50.0
18	7{1,12}	Me	5-Me	0.23	21.9	7.4	50.0
19	7{1,13}	Cl	3-Cl	0.94	50.00	30.0	50.0
20	7{1,14}	Cl	4-Cl	0.44	50.00	37.3	50.0
21	7{1,15}	Cl	5-Cl	0.25	50.00	38.1	50.0
22	7{1,16}	OMe	3-OMe	2.75	50.00	35.9	50.0
23	7{1,17}	OMe	4-OMe	0.32	50.00	50.0	50.0
24	7{1,18}	OMe	5-OMe	0.42	28.60	9.5	50.0
25	7{1,19}	OMe	5-Cl	0.45	50.0	29.4	33.4



entry	library member	R ¹	R ²	IC ₅₀ (μM)			
				Mn(II)	Co(II)	Fe(II)	Ni(II)
26	7{2,11}	Me	3-Me	3.38	50.0	50.0	50.0
27	7{2,12}	Me	5-Me	1.18	35.7	40.0	50.0
28	7{2,13}	Cl	3-Cl	1.48	50.0	46.0	50.0
29	7{2,14}	Cl	4-Cl	4.4	50.0	38.7	50.0
30	7{2,15}	Cl	5-Cl	1.1	50.0	34.0	50.0
31	7{2,17}	OMe	4-OMe	8.89	9.9	7.7	28.0
32	7{2,18}	OMe	5-OMe	4.6	50	9.7	10.6
33	7{2,19}	OMe	5-Cl	5.72	50.0	50.0	50.0

with MetAP–Mn(II) via the comparative binding energy (COMBINE) method.²⁵ To do so, one pose was selected for each ligand according to the criteria of (a) a low AutoDock

free-energy score and (b) a structurally-consistent orientation as defined by requiring close contact between the ligand carboxyl/carboxylate group and the receptor metal ion. The

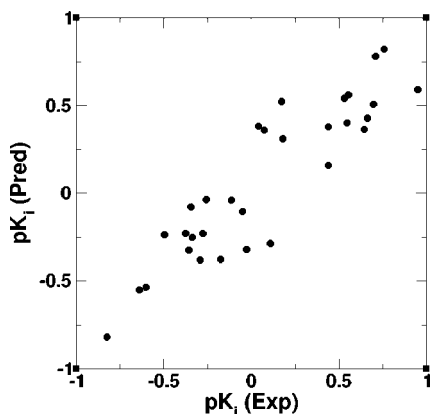


Figure 4. Comparison of ($\log[\text{IC}_{50} (\mu\text{M})]$) values predicted via the COMBINE model versus the corresponding experimental training data for furan- and thiophene-carboxylate ligands binding to MetAP–Mn(II).

resulting ligand-residue van der Waals and electrostatic terms were then trained to reproduce our $\log(\text{IC}_{50})$ affinity data (see Tables 2 and 3) via partial least-squares (PLS) analysis using the Simca-P software.²⁶ The models were refined iteratively by replacement of misaligned poses (identified as outliers in interim plots of predicted vs experimental IC_{50} values) with more appropriate structures that generally exhibited poorer AutoDock scores but closer adherence to structural-consistency criterion. In cases where all docked poses yielded an outlier result, the molecule was eliminated from consideration.

On the basis of the COMBINE modeling methodology, we were unable to achieve a statistically-significant model for the observed IC_{50} values of free-acid forms of compounds ($7\{1,2-19\}$, $7\{2,1-7,11-15,17-19\}$) interacting with MetAP–Mn(II) without discarding a substantial fraction of the total training set. However, for the carboxylate manifold, a strongly-correlating and internally-predictive model was achieved for a ligand manifold that included 31 of the 33 ligands, omitting only molecules ($7\{1,4\}$, $7\{2,6\}$). Predicted $\log(\text{IC}_{50})$, shown graphically in Figure 4, reproduce experimental values with a correlation coefficient of $R^2 = 0.82$ and exhibited a leave-one-out cross-validated correlation of $Q^2 = 0.62$. The relative success of the carboxylate model and failure of the free acids in reproducing the experiment suggests that the bioactive form of these molecules is likely the carboxylate, a conjecture that is supported by computed pK_a values (as obtained via the ChemAxon pK_a plug-in)²⁷ that are uniformly below 3.2 for the furan-based ligands and below 3.4 for the thiophenes.

Visualization of the full manifold of 31 ligands docked within the MetAP–Mn(II) receptor, as is depicted in Figure 5, provides important pharmacophoric insight. One notes that the interaction best conserved across the manifold is the ionic coupling between the carboxylate and the top Mn(II) ion (Mn 901 according to the crystal structure residue numbering), which agrees with prior crystallographic observations and a related ligand⁹ and is likely a key factor in dictating the complex structure. The lower metal ion (Mn 902) does not appear to be positioned favorably for ionic coupling with the carboxylate, although it may engage in tangible van der Waals interactions with the furan/thiophene group. Several

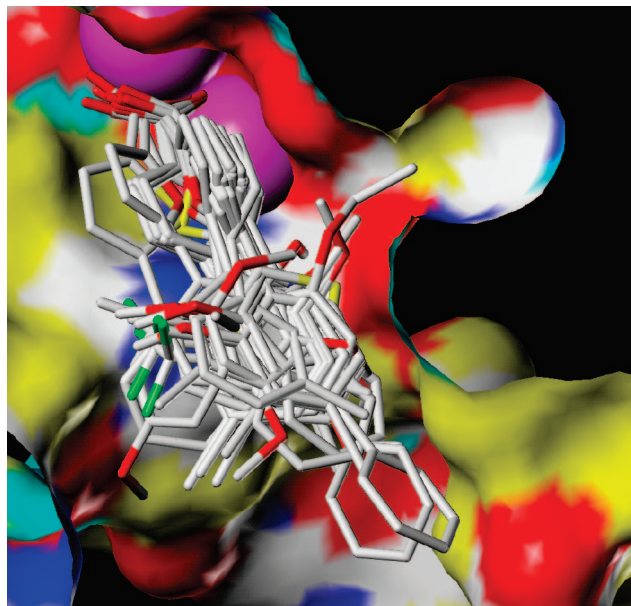


Figure 5. Ensemble of furan- and thiophene-carboxylate ligands in their predicted conformations in complex with the MetAP–Mn(II) receptor. Ligands are colored according to standard CPK colors (C = white, O = red, halide = green, S = yellow), whereas the receptor surface is rendered according to prospective pharmacophore features (yellow = hydrophobic, red = acceptor O, blue = acceptor N, cyan = donatable H, white = other polar). The Mn(II) ions are rendered as magenta space-filling spheres.

receptor hydrophobic features appear to be available for coupling, including a surface (Tyr 62 + Phe 177) near Mn 901 (mostly above the plane depicted in Figure 5) and two patches around the receptor periphery (Cys 169 + Tyr 168). A pair of H-bond acceptor sites are available (Gly170 and Glu 204), as well as a trio of donors that includes the imidazole side chains of His 79 and His 178 and the backbone amide of Cys 169. Structurally, the ligand manifold appears to conserve the orientation of the furan/thiophene heteroatom (i.e., O or S, respectively) primarily toward His 178, with only minor variations in the angle with respect to the carboxylate. Substantial variations are observed in the relative orientation of the ligands' terminal hydrophobic group, likely, because of the diversity of chemical functionality on this group across the library.

Beyond helping us to rationalize plausible docked conformers, the COMBINE methodology provides a means for systematic identification of those ligand–receptor interactions that make the greatest contribution to receptor selectivity, in that both the magnitude and signs of the COMBINE coefficients provide key insight into trends governing the observed ligand efficacy. Specifically, positive COMBINE coefficients correspond to residues whose favorable interactions with ligands correlate directly with favorable observed binding affinity, while those with negative coefficients have predicted ligand interactions that are inversely correlated with favorable binding affinities. Examples of the latter include residues that can hinder ligands from adopting another bound conformer of greater stability or those whose modeled structure is somehow inaccurate, such as residues with substantial conformation variability that is not represented in the static crystal structure model or residues modeled in

Table 4. Key residues for ligand binding as determined by reasonable proximity to the receptor (at least one atom within 5.0 Å from the cocrystallized ligand) and large COMBINE contributions (top ten, as ranked by coefficient energy)

positive van der Waals		negative van der Waals		positive electrostatic		negative electrostatic	
residue	coefficient	residue	coefficient	residue	coefficient	residue	coefficient
His 79	0.031	Gly 170	-0.024	Gly 170	0.025	His 178	-0.047
Cys 169	0.024	His 171	-0.019	Asp 97	0.022	His 171	-0.030
His 178	0.015	Phe 177	-0.013	Cys 169	0.025	Mn 901	-0.011
Mn 901	0.009	Asp 108	-0.003	Thr 99	0.016	Asp 108	-0.006
Tyr 168	0.008	Mn 902	-0.001	Glu 235	0.006		
				Mn 902	0.006		

the wrong protonation state. A summary of key receptor residue coefficients is provided in Table 4, along with a graphical representation in Figure 6.

An SAR analysis of this library revealed that the thiophene analogs generally had reduced potencies relative to their furan analogs. Two possible rationalizations appear quite obvious from our COMBINE model: the thiophene S heteroatom, sterically larger than the furan O atom, generally sits in a sterically-rather-unfavorable region as indicated by the negative COMBINE van der Waals coefficients on Mn 902, His 171, and Phe 177. Furthermore, the docked conformers for many of the thiophene ligands, such as **7**{2,17} (see Figure 6B), tend to approach the upper metal (e.g., Mn 901) to within distances less than the van der Waals radius, thus leading to a steric clash. The fact that all library members except **7**{2,17} showed preference for the Mn(II)-form of the enzyme relative to the larger metals (Co(II), Fe(II), Ni(II)), together with the observation of poorer affinity for larger thiophenes, provides further evidence that the region of the metal ions may constitute a steric bottleneck, such that any increase in either ligand or receptor bulk may either infringe on the sterically-undesirable Mn 902 surface or

approach too closely to Mn 901, thereby detracting from affinity relative to that of a furoic acid coupling with MetAP-Mn(II). Furthermore, because Mn 901 has a negative electrostatic coefficient, its cationic attraction for the ligand carboxyl group may be less favorable than that of Mn 902. Thus, the fact that the carboxyl on thiophene ligands tends to interact primarily with the upper (likely less favorable) metal, whereas the furoic acids interact closely with the lower metal both via their carboxyl and via the furan oxygen provides further rationale for generally-better affinity of the furoic species.

In the exploration of a range of chemical functionality among the R¹ and R² substituent groups, we determined that the receptor is capable of tolerating a reasonably diverse collection of hydrophobic groups attached to the furan/thiophene moiety without great loss of affinity. Among the various substituted phenyls, compounds **7**{1,2-5} and **7**{1,11-15,17-19} displayed potencies in low submicromolar range (0.15-0.94) and had very high selectivity toward the Mn(II) form of the enzyme (100-300-fold). Replacement of the phenyl ring by different aromatic rings altered the potencies to various extents but did not affect the selectivities.

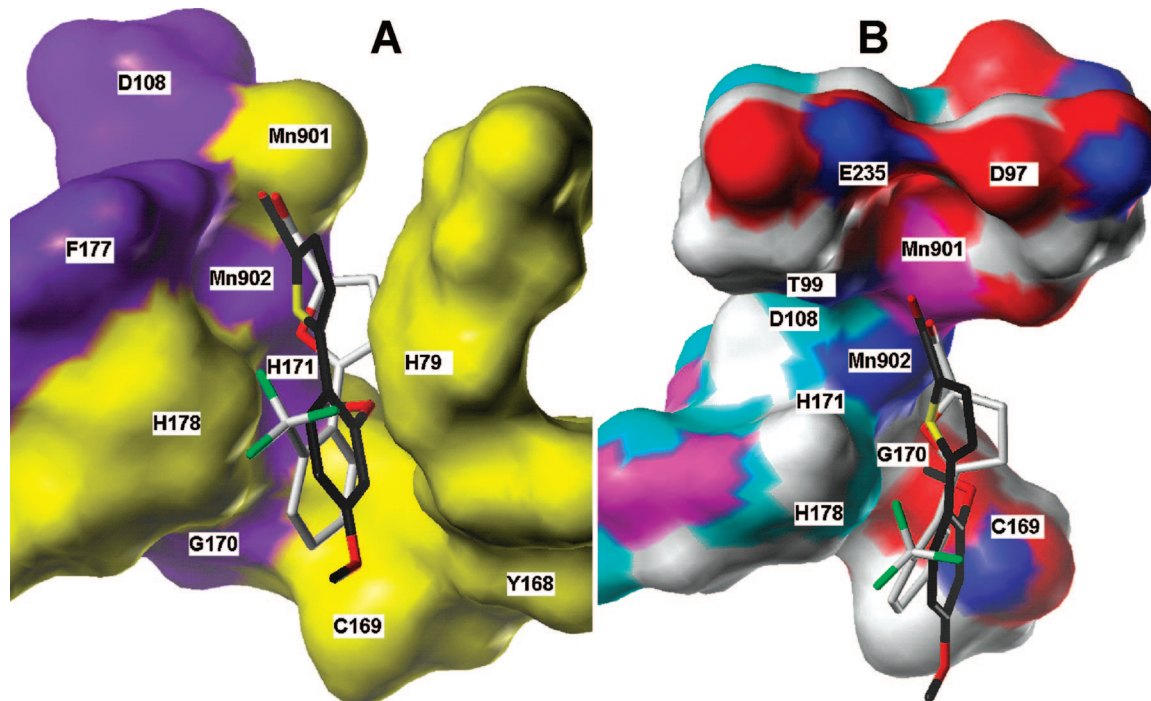


Figure 6. Top-scoring (light grey sticks) and bottom-scoring (black) ligands drawn relative to the positions of receptor residues exhibiting key van der Waals (A) and electrostatic (B) interactions. In case A, gold surfaces indicate residues with positive COMBINE coefficients, whereas purple surfaces are negative. In case B, red and blue surfaces reflect electronegative and electropositive surfaces with positive COMBINE coefficients, whereas cyan and magenta correspond to electronegative and electropositive surfaces with negative COMBINE coefficient.

Incorporation of 1*H* indole was favorable (entry 7), which might be explained by formation of an H-bond with the backbone carbonyl of Gly 170. Naphthyl and biphenyl are also tolerated (entries 5 and 6), although thiophenyl and benzo thiophenyl seemed to be unfavorable (entries 8 and 9). Interestingly, the CF₃ analog of both the furan and thiophene series showed high enzyme inhibition activity and high selectivity (entries 4 and 14). Our COMBINE analysis suggests that this is likely caused by the favorable van der Waals coupling between the CF₃ group and its most proximate receptor groups including the sterically favorable His 79 (Table 4, column 1) and His 178 species. The large negative electrostatic coefficient on His 178 further suggests that the face it orients toward the CF₃ group, which would have been the electronegative/acidic N_ε side of the imidazole, actually correlates to favorable interactions with electronegative groups such as CF₃. This suggests that either the N_ε may be protonated in this case or that the imidazole is capable of a low-barrier rotation to place the N_δ in line with the CF₃. Alkoxy groups proved to be less effective in exploiting these interactions, likely, because of the alkoxy oxygen being further up the molecule (i.e., closer to the carboxylate) than the CF₃ fluorines and thus less able to reach the imidazole groups. Sequential shifting of the positions of the substituents on the phenyl rings (i.e., 2,3, 2,4-, and 2,5-) altered the potencies. More specifically, the 2,3- and 2,4-substituted pattern in the furoic acid and the thiophene carboxylic acids series seems to be particularly unfavorable, especially for polar substituents (e.g., entries 22 and 31). The apparent explanation derived from our *in silico* analysis is that ligands with such substitution patterns tend to be forced by sterics to orient their electronegative alkoxy oxygens toward the Gly 170 backbone carbonyl. Not only does this induce an intuitive electrostatic clash, but Gly 170 has the largest positive COMBINE coefficient of all receptor residues, indicating a specific preference for electropositive groups. Furthermore, Gly 170 also has the largest negative van der Waals coefficient, reflecting substantial unfavorability toward hydrophobic interactions. The relative success of the 2,5-substituted ligands appears to arise from their ability to reorient their ring to establish distance between the 2-substituent and the unfavorable Gly 170 environment.

In the comparison of the relative disposition of our best, 7{1,5}, and worst, 7{2,17}, inhibitors, Figure 6 provides a reasonable study in how to derive the most and least out of a MetAP ligand. Molecule 7{2,17} suffers from unfavorable steric contacts with Mn 902, Gly 170, Asp 108, and Phe 177. The relatively large size of the thiophene may also induce an overly close contact with the otherwise favorable Mn 901. Conversely, 7{1,5} exploits favorable van der Waals coupling with Mn 901, His 79, and His 178 and also engages in productive electrostatic interactions that 7{2,17} lacks, including those with Mn 902, His 171, and His 178. Some prospects for improving the latter may exist, however. Tyr 168, for example, provides a favorable hydrophobic surface that 7{1,5} does not exploit, and Cys 169 also provides an important lipophile that benefits only the biphenyls (7{1,7} and 7{2,7}). Permutation of the 2-CF₃ substituent with other groups at other positions on the phenyl might enhance the

net ligand affinity. Another potential mode of refinement may lie in judicious incorporation of ligand H-donor groups capable of interacting with the various receptor acceptors sites, such as the Glu 204 carboxylate and the Gly 170 backbone carbonyl, although these groups both lie in areas that are sterically limited and thus not very amenable to any but the smallest substituent groups. The Cys 169 backbone amide N-H group may also prove to be a useful target.

The compounds reported herein were evaluated *in silico* according to standard oral availability and absorption–distribution–metabolism–excretion (ADME) criteria, using SYBYL²⁸ and VolSurf,²⁹ respectively. These compounds are Lipinski-compliant, tend toward BBB permeability (a possible problem), good CACO2 permeability, moderate-to-good solubility, have moderate-to-good albumin-transport properties, are typically not hERG blocking threats, and have moderate metabolic stability; however many of these are predicted to have poor volume distribution. Chemical diversity analysis relative to the PubChem collection (as performed via Diverse Solutions)³⁰ suggests that the present collection contain some pockets of relatively diverse compounds. In essence, the collection appears to be reasonably drug-like; however some efforts would be expended in any subsequent lead-refinement stage toward improvement of delivery issues.

Conclusion

In summary we have developed a new strategy for the generation of methionine aminopeptidase inhibitors. This method involves immobilization of the acid on PS-BEMP, Suzuki coupling and subsequent release to afford the products in moderate yields and excellent purities. Biological evaluation on the Co(II)-, Mn(II)-, Ni(II)- and the Fe(II)- forms of EcMetAP and subsequent computational studies provided valuable information in determining the structural elements responsible for potency. Ionic interaction between Mn(II) ion and the carboxylate group of MetAP ligand dictate potency and metalloform selectivity. Judicious incorporation of H-bond donors and acceptors within the ligand provide sites for interaction for various receptor sites.

Experimental Section

General Experimental Methods. All chemicals and resins were used as purchased from commercial suppliers. Solvents such as methylene chloride and ether were dried bypassing through two packed columns of neutral alumina using the PurSolv solvent purification system (Innovative Technology, Inc.). DMF and DMSO (HPLC grade) were degassed with argon before use. Reactions with air-sensitive materials were carried out with oven-dried glassware under a stream of dry argon using standard syringe techniques. Reactions (immobilization, release step, and wash sequences) were carried out in 10 mL glass–fritted tubes fitted onto Miniblock Synthesizers (24-array) on a Brunswick Scientific's Bodhan 2080 shaking/washing station. Microwave reactions were done in an automated Emrys single-mode microwave reactor, and the vials (0.5–2.0 mL) were purchased from Biotage. Parallel evaporation was performed on the GeneVac EZ-2 Plus evaporator system. PrepSep silica gel SPE cartridges

obtained from Fisher Scientific were used for filtration. Thin layer chromatography was performed on silica gel 60F254 plates (EM-5717, Merck). Deuterated solvents were purchased from Cambridge Isotope laboratories. ^1H and ^{13}C spectra were recorded on a Bruker DRX-400 spectrometer operating at 400 and 100 MHz, respectively, or on a Bruker Avance operating at 500 and 125 MHz, respectively. Chemical shifts are reported in parts per million (ppm) downfield from TMS (0 ppm). Data are reported as follows: chemical shift, multiplicity (app = apparent, s = singlet, d = doublet, t = triplet, q = quartet, dd = doublet of doublets, m = multiplet, br = broad), coupling constants, and integration. Chemical shifts are reported in parts per million (ppm) downfield from TMS, using the middle resonance of CDCl_3 (77.2 ppm) as an internal standard. HPLC analyses were carried out at the KU-CMLD Core C laboratory using a Xterra MS C-18 column (5 μm , 4.6 \times 150 mm) and a gradient elution (10% CAN-water to 100% ACN) on a Waters mass-directed fractionation instrument using a Waters 2767 sample manager, Waters 2525 HPLC pump, a 2487 dual λ absorbance detector, and Waters/Micromass ZQ (quadrupole) MS ELSD detector (Sedex 85) connected to a PC with MassLynx workstation. High-resolution mass spectra (HRMS) [ESI+] were obtained using Waters/Micromass LCT Premier (TOF instrument).

Immobilization Step. To a Bodhan MiniBlock Synthesizer (24 array), fitted with glass-fritted 10 mL tubes, was added a mixture of degassed DMSO/DMF (1:1) and the resin PS-BEMP (0.5 g, 2.2 mmol/g). The reaction mixture was shaken for one hour on the Bodhan shaking/washing station. Acids **2**{1,2} (1.5 equiv) were added, and the reaction mixture was shaken at 60 °C overnight. Filtration of the resin, sequential washes with DCM/MeOH (3 \times), followed by Et_2O , provided the resin-bound acid intermediate **5**. An aliquot sample of every batch of resin-bound intermediates **5** was cleaved with HCl to determine the amount of acid immobilized on the resin, which corresponded to ~56% loading of the resin.

General Procedure for Suzuki Reactions for Substrates 3{1,2,1-19}. An oven-dried microwave vial was charged with resin-bound acid intermediates **5**{1,2}, boronic acids **3**{1-19} (4 equiv), and DMF (0.017 M). Catalysts $\text{Pd}(\text{PPh}_3)_2\text{Cl}_2$ or $\text{Pd}(\text{PPh}_3)_4$ (15 mol) and bases K_2CO_3 or K_3PO_4 (5 equiv) were added to the respective reaction mixtures using the MiniBlock resin dispenser (calibrated, respectively). The reaction vial was sealed, flushed with argon, and irradiated in a microwave reactor at 120 °C for 5 min. Filtration of the reaction mixture through 10 mL glass-fritted tubes and sequential washing with DCM/MeOH (3 \times), followed by Et_2O , provided the resin-bound acid intermediate **6** ready for the subsequent cleavage step. For substrates **3**{1-4,6,7,12-19}, the combination of $\text{Pd}(\text{PPh}_3)_2\text{Cl}_2/\text{K}_2\text{CO}_3$ was used. For substrates **3**{5,8-11}, the combination of $\text{Pd}(\text{PPh}_3)_4/\text{K}_3\text{PO}_4$ was used.

Cleavage Step. To the resin **6** in DCM (1 mL) was added 4 equiv of HCl in dioxane (4 N), and the reaction was shaken at RT (room temperature) for 3 h. Filtration through PrepSep silica gel SPE cartridges, followed by evaporation in an EZ-Genevac Plus Parallel Evaporator, provided the products,

which were analyzed at 215 nm by RP HPLC-MS-UV. The compounds were purified by preparative HPLC (purities reported below) before determining inhibitory activity.

Enzyme Inhibition Assays. Recombinant *E. coli* MetAP1 was purified as an apoenzyme as reported previously.²⁰ All compounds were placed on 384-well flat-bottom polystyrene microplate in 12 concentrations in 2 fold dilutions starting from 50 μM (final concentration). Serial dilutions were performed by Precision 2000 automated microplate pipetting system (BioTek Instruments Inc., Winooski, VT). The assay mixture (80 μL final volume) contains 20 μL of compound, 50 mM MOPS (pH 7.0), 1.0 μM apo-EcMetAP, 200 μM Met-AMC (Bachem Bioscience Inc., King of Prussia, PA), and 100 μM MnCl_2 . Enzymatic activity of MetAP was monitored by a fluorescence kinetic assay using Met-AMC as a fluorogenic substrate on a SpectraMax Gemini XS microplate fluorescence reader (Molecular Devices Corp., Sunnyvale, CA) (λ_{ex} = 360 nm, λ_{em} = 460 nm); 2.5% DMSO was used as a negative control, while compound **7**{1,2} was used as a positive control. The IC_{50} values were obtained from nonlinear curve fitting of the plot of percent inhibition versus inhibitor concentration $[I]$ using the equation, %inhibition = $100/\{1 + (\text{IC}_{50}/[I])^k\}$, where k is the Hill coefficient.

Spectroscopic and Analytical Data. 5-(2-Methylphenyl)furan-2-carboxylic Acid 7{1,1}. Purity: 99%. ^1H NMR (400 MHz, CDCl_3): δ 7.78 (m, 1H), 7.42 (d, J_{HH} = 3.2 Hz, 1H), 7.29–7.25 (m, 3H), 7.69 (d, J_{HH} = 3.2 Hz, 1H), 2.54 (s, 3H). ^{13}C NMR (125 MHz, CDCl_3): δ 162.7, 158.6, 142.3, 135.7, 131.4, 129.1, 128.7, 128.1, 126.2, 121.7, 110.6, 21.7. HRMS Calcd for $\text{C}_{12}\text{H}_{10}\text{O}_3$: (M – H)⁺ 201.0552. Found: 201.0555.

5-(2-Methoxyphenyl)furan-2-carboxylic Acid 7{1,3}. Purity: 94%. ^1H NMR (400 MHz, CDCl_3): δ 8.03 (d, J_{HH} = 7.7 Hz, 1H), 7.42–7.32 (m, 2H), 7.08–7.04 (m, 2H), 6.99 (d, J_{HH} = 8.2 Hz, 1H), 3.96 (s, 3H). ^{13}C NMR (125 MHz, CDCl_3): δ 162.8, 156.4, 155.2, 141.5, 130.1, 127.2, 122.3, 120.9, 118.2, 112.1, 111.0, 55.5. HRMS Calcd for $\text{C}_{12}\text{H}_{10}\text{O}_4$: (M – H)⁺ 217.0501. Found: 217.0491.

5-(2-Ethoxyphenyl)furan-2-carboxylic Acid 7{1,4}. Purity: 100%. ^1H NMR (400 MHz, CDCl_3): δ 8.04 (d, J_{HH} = 7.5 Hz, 1H), 7.41 (br s, J_{HH} = 3.2 Hz, 1H), 7.31–7.29 (m, 1H), 7.12 (br s, J_{HH} = 3.2 Hz, 1H), 7.04 (m, 1H), 6.96 (d, J_{HH} = 8.0 Hz, 1H), 4.18 (d, J_{HH} = 6.8 Hz, 2H), 1.55 (t, J_{HH} = 6.8 Hz, 3H). ^{13}C NMR (125 MHz, CDCl_3): δ 163.0, 155.8, 155.4, 141.4, 130.1, 127.2, 122.3, 120.7, 118.2, 112.1, 111.8, 64.0, 14.9. HRMS Calcd for $\text{C}_{13}\text{H}_{12}\text{O}_4$: (M – H)⁺ 231.0658. Found: 231.0653.

5-(4-Methylnaphthalen-1-yl)furan-2-carboxylic Acid 7{1,6}. Purity: 99%. ^1H NMR (400 MHz, CDCl_3): δ 8.40 (br s, 1H), 8.07 (br s, 1H), 7.75 (d, J_{HH} = 7.2 Hz, 1H), 7.6–7.5 (m, 3H), 7.39 (d, J_{HH} = 7.2 Hz, 1H), 6.83 (d, J_{HH} = 3.2 Hz, 1H), 2.75 (s, 3H). ^{13}C NMR (125 MHz, CDCl_3): δ 163.0, 158.7, 142.9, 136.8, 132.9, 130.3, 127.2, 126.8, 126.2, 126.1, 125.5, 125.4, 124.7, 121.8, 111.3, 19.8. HRMS Calcd for $\text{C}_{16}\text{H}_{12}\text{O}_3$: (M – H)⁺ 251.0708. Found: 251.0708.

5-(2,3-Dimethylphenyl)furan-2-carboxylic Acid 7{1,11}. Purity: 98%. ^1H NMR (400 MHz, CDCl_3): δ 7.50 (d, J_{HH} = 6.8 Hz, 1H), 7.42 (s, 1H), 7.19 (br s, 2H), 6.62 (s, 1H), 2.39

(s, 3H), 2.35 (s, 3H). ^{13}C NMR (125 MHz, CDCl_3): δ 163.1, 159.4, 142.5, 137.2, 134.8, 131.0, 129.4, 126.9, 125.6, 121.6, 111.0, 20.7, 17.1. HRMS Calcd for $\text{C}_{13}\text{H}_{12}\text{O}_3$: $(\text{M} - \text{H})^+$ 215.0708. Found: 215.0711.

5-(2,3-Dichlorophenyl)furan-2-carboxylic Acid 7{1,13}. Purity: 100%. ^1H NMR (400 MHz, $\text{DMSO}-d_6$): δ 7.83 (d, $J_{\text{HH}} = 8.0$ Hz, 1H), 7.71 (d, $J_{\text{HH}} = 8.0$ Hz, 1H), 7.50 (app. t, $J_{\text{HH}} = 8.0$ Hz, 1H), 7.35 (d, $J_{\text{HH}} = 3.5$ Hz, 1H), 7.29 (d, $J_{\text{HH}} = 3.5$ Hz, 1H). ^{13}C NMR (125 MHz, $\text{DMSO}-d_6$): δ 159.1, 151.6, 144.8, 133.2, 130.7, 129.8, 128.7, 128.1, 127.6, 119.1, 113.6. HRMS Calcd for $\text{C}_{11}\text{H}_6\text{Cl}_2\text{O}_3$: $(\text{M} - \text{H})^+$ 254.9616, $(\text{M} + 1)^+$ 256.9602, $(\text{M} + 3)^+$ 258.9584. Found: 254.9631 $(\text{M} - \text{H})^+$.

5-(2,4-Dichlorophenyl)furan-2-carboxylic Acid 7{1,14}. Purity: 100%. ^1H NMR (400 MHz, $\text{DMSO}-d_6$): δ 7.88 (d, $J_{\text{HH}} = 8.5$ Hz, 1H), 7.80 (d, $J_{\text{HH}} = 2.0$ Hz, 1H), 7.59 (app. dd, $J_{\text{HH}} = 8.4, 2.0, 2.4$ Hz, 1H), 7.36 (d, $J_{\text{HH}} = 3.6$ Hz, 1H), 7.27 (d, $J_{\text{HH}} = 3.6$ Hz, 1H). ^{13}C NMR (125 MHz, $\text{DMSO}-d_6$): δ 156.6, 131.5, 128.4, 128.0, 127.5, 125.7, 124.1, 116.9, 110.8. HRMS Calcd for $\text{C}_{11}\text{H}_6\text{Cl}_2\text{O}_3$: $(\text{M} - \text{H})^+$ 254.9616, $(\text{M} + 1)^+$ 256.9581, $(\text{M} + 3)^+$ 258.9579. Found: 254.9611 $(\text{M} - \text{H})^+$.

5-(2,5-Dichlorophenyl)furan-2-Carboxylic Acid 7{1,15}. Purity: 100%. ^1H NMR (400 MHz, $\text{DMSO}-d_6$): δ 7.78 (br s, 1H), 7.66 (d, $J_{\text{HH}} = 8.5$ Hz, 1H), 7.52 (br d, $J_{\text{HH}} = 8.5$ Hz, 1H), 7.37 (d, $J_{\text{HH}} = 3.3$ Hz, 1H), 7.33 (d, $J_{\text{HH}} = 3.3$ Hz, 1H). ^{13}C NMR (125 MHz, $\text{DMSO}-d_6$): δ 159.0, 150.8, 144.8, 132.6, 132.3, 129.8, 128.9, 128.7, 127.7, 119.2, 113.6. HRMS Calcd for $\text{C}_{11}\text{H}_6\text{Cl}_2\text{O}_3$: $(\text{M} - \text{H})^+$ 254.9616, $(\text{M} + 1)^+$ 256.9594, $(\text{M} + 3)^+$ 258.9587. Found: 254.9621.

5-(2,3-Dimethoxyphenyl)furan-2-carboxylic Acid 7{1,16}. Purity: 98%. ^1H NMR (400 MHz, CDCl_3): δ 7.58 (d, $J_{\text{HH}} = 7.9$ Hz, 1H), 7.42 (d, $J_{\text{HH}} = 3.4$ Hz, 1H), 7.16–7.12 (m, 2H), 6.94 (d, $J_{\text{HH}} = 8.1$ Hz, 1H), 3.91 (s, 3H), 3.88 (s, 3H). ^{13}C NMR (125 MHz, CDCl_3): δ 161.5, 154.9, 153.1, 146.4, 141.7, 124.4, 123.4, 122.2, 118.9, 113.0, 111.9, 60.0, 55.9. HRMS Calcd for $\text{C}_{13}\text{H}_{12}\text{O}_5$: $(\text{M} - \text{H})^+$ 247.0607. Found: 247.0610.

5-(2,4-Dimethoxyphenyl)furan-2-carboxylic Acid 7{1,17}. Purity: 99%. ^1H NMR (400 MHz, $\text{DMSO}-d_6$): δ 7.7 (d, $J_{\text{HH}} = 8.3$ Hz, 1H), 7.26 (d, $J_{\text{HH}} = 3.5$ Hz, 1H), 6.87 (d, $J_{\text{HH}} = 3.5$ Hz, 1H), 6.68–6.66 (m, 2H), 3.9 (s, 3H), 3.81 (s, 3H). ^{13}C NMR (125 MHz, $\text{DMSO}-d_6$): δ 161.0, 159.2, 157.2, 153.3, 142.2, 131.4, 119.9, 110.8, 109.8, 105.8, 98.7, 55.7, 55.4. HRMS Calcd for $\text{C}_{13}\text{H}_{12}\text{O}_5$: $(\text{M} - \text{H})^+$ 247.0607. Found: 247.0601.

5-(2,5-Dimethoxyphenyl)furan-2-carboxylic Acid 7{1,18}. Purity: 100%. ^1H NMR (400 MHz, CDCl_3): δ 7.56 (d, $J_{\text{HH}} = 2.4$ Hz, 1H), 7.41 (d, $J_{\text{HH}} = 3.6$ Hz, 1H), 7.10 (d, $J_{\text{HH}} = 3.6$ Hz, 1H), 6.90 (d, $J_{\text{HH}} = 4.4$ Hz, 2H), 3.91 (s, 3H), 3.85 (s, 3H). ^{13}C NMR (125 MHz, CDCl_3): δ 162.3, 155.0, 153.7, 150.9, 141.5, 122.3, 118.7, 115.9, 112.4, 112.3, 111.8, 56.0. HRMS Calcd for $\text{C}_{13}\text{H}_{12}\text{O}_5$: $(\text{M} - \text{H})^+$ 247.0607. Found: 247.0603.

5-(2-Methyl)thiophene-2-carboxylic Acid 7{2,1}. Purity: 96%. ^1H NMR (400 MHz, CDCl_3): δ 7.87 (d, $J_{\text{HH}} = 3.6$ Hz, 1H), 7.41 (d, $J_{\text{HH}} = 7.2$ Hz, 1H), 7.29–7.24 (m, 3H), 7.09 (d, $J_{\text{HH}} = 3.2$ Hz, 1H), 2.43 (s, 3H). ^{13}C NMR (125 MHz, CDCl_3): δ 167.6, 152.2, 136.1, 135.1, 133.0, 131.8,

131.6, 131.0, 128.9, 127.5, 126.2, 21.2. HRMS Calcd for $\text{C}_{12}\text{H}_{10}\text{O}_2\text{S}$: $(\text{M} - \text{H})^+$ 217.0324. Found: 217.0332.

5-(2-Methoxyphenyl)thiophene-2-carboxylic Acid 7{2,3}. Purity: 100%. ^1H NMR (400 MHz, CDCl_3): δ 7.85 (br s, 1H), 7.72 (d, $J_{\text{HH}} = 6.8$ Hz, 1H), 7.51 (br s, 1H), 7.34 (br d, $J_{\text{HH}} = 7.3$ Hz, 1H), 7.02 (br d, $J_{\text{HH}} = 8.0$ Hz, 2H), 3.98 (s, 3H). ^{13}C NMR (125 MHz, CDCl_3): δ 166.9, 155.9, 147.9, 145.5, 131.2, 129.9, 128.3, 125.5, 122.1, 121.0, 111.7, 55.6. HRMS Calcd for $\text{C}_{12}\text{H}_{10}\text{O}_3\text{S}$: $(\text{M} - \text{H})^+$ 233.0273. Found: 233.0269.

5-(2-Ethoxyphenyl)thiophene-2-carboxylic Acid 7{2,4}. Purity: 96%. ^1H NMR (400 MHz, CDCl_3): δ 7.86 (d, $J_{\text{HH}} = 4.4$ Hz, 1H), 7.73 (br d, $J_{\text{HH}} = 8.0$ Hz, 1H), 7.53 (d, $J_{\text{HH}} = 4.4$ Hz, 1H), 7.32 (br t, $J_{\text{HH}} = 7.8$ Hz, 1H), 7.03–6.99 (m, 2H), 4.22 (q, $J_{\text{HH}} = 6.8$ Hz, 2H), 1.57 (t, $J_{\text{HH}} = 7.0$ Hz, 3H). ^{13}C NMR (125 MHz, CDCl_3): δ 167.5, 155.2, 148.2, 134.5, 131.5, 129.8, 128.3, 125.4, 122.1, 120.8, 112.4, 64.6, 14.8. HRMS Calcd for $\text{C}_{13}\text{H}_{12}\text{O}_3\text{S}$: $(\text{M} - \text{H})^+$ 247.0429. Found: 247.0459.

5-(2-(Trifluoromethyl)phenyl)thiophene-2-carboxylic Acid 7{2,5}. Purity: 100%. ^1H NMR (400 MHz, CDCl_3): δ 7.85 (d, $J_{\text{HH}} = 4.0$ Hz, 1H), 7.80 (d, $J_{\text{HH}} = 7.64$ Hz, 1H), 7.62 (m, 3H), 7.15 (d, $J_{\text{HH}} = 4.0$ Hz, 1H). ^{13}C NMR (125 MHz, CDCl_3): δ 166.9, 148.3, 134.7, 132.9, 132.2, 131.6, 129.5, 128.9, 126.4, 124.8, 122.6, 120.4. HRMS Calcd for $\text{C}_{12}\text{H}_7\text{F}_3\text{O}_2\text{S}$: $(\text{M} - \text{H})^+$ 271.0041. Found: 217.0059.

5-(2,3-Dimethylphenyl)thiophene-2-carboxylic Acid 7{2,11}. Purity: 98%. ^1H NMR (400 MHz, CDCl_3): δ 7.86 (d, $J_{\text{HH}} = 3.7$ Hz, 1H), 7.52–7.12 (m, 3H), 7.09 (d, $J_{\text{HH}} = 3.7$ Hz, 1H), 2.34 (s, 3H), 2.29 (s, 3H). ^{13}C NMR (125 MHz, CDCl_3): δ 167.1, 152.9, 137.8, 135.05, 135.04, 133.3, 131.7, 130.5, 128.4, 127.6, 125.5, 20.8, 17.1. HRMS Calcd for $\text{C}_{13}\text{H}_{12}\text{O}_2\text{S}$: $(\text{M} - \text{H})^+$ 231.04801. Found: 231.0477.

5-(2,5-Dimethylphenyl)thiophene-2-carboxylic Acid 7{2,12}. Purity: 97%. ^1H NMR (400 MHz, CDCl_3): δ 7.86 (d, $J_{\text{HH}} = 3.2$ Hz, 1H), 7.25–7.08 (m, 4H), 2.39 (s, 3H), 2.35 (s, 3H). ^{13}C NMR (125 MHz, CDCl_3): δ 166.9, 152.5, 135.7, 135.1, 132.9, 132.7, 131.5, 131.0, 130.9, 129.6, 127.4, 20.8, 20.6. HRMS Calcd for $\text{C}_{13}\text{H}_{12}\text{O}_2\text{S}$: $(\text{M} - \text{H})^+$ 231.04801. Found: 231.0473.

5-(2,3-Dimethoxyphenyl)thiophene-2-carboxylic Acid 7{2,16}. Purity: 100%. ^1H NMR (400 MHz, CDCl_3): δ 7.81 (d, $J_{\text{HH}} = 4.0$ Hz, 1H), 7.62 (d, $J_{\text{HH}} = 8.4$ Hz, 1H), 7.39 (d, $J_{\text{HH}} = 4.0$ Hz, 1H), 6.58–6.54 (m, 2H), 3.95 (s, 3H), 3.82 (s, 3H). ^{13}C NMR (125 MHz, CDCl_3): δ 167.3, 153.4, 147.2, 146.0, 134.5, 132.5, 1219.1, 128.5, 127.0, 119.6, 112.5, 60.2, 55.9. HRMS Calcd for $\text{C}_{13}\text{H}_{12}\text{O}_4\text{S}$: $(\text{M} - \text{H})^+$ 263.0378. Found: 263.0400.

5-(2,4-Dimethoxyphenyl)thiophene-2-carboxylic Acid 7{2,17}. Purity: 100%. ^1H NMR (400 MHz, CDCl_3): δ 7.82 (d, $J_{\text{HH}} = 9.6$ Hz, 1H), 7.62 (d, $J_{\text{HH}} = 8.4$ Hz, 1H), 7.39 (d, $J_{\text{HH}} = 4.0$ Hz, 1H), 6.58–6.54 (m, 2H), 3.88 (s, 3H), 3.82 (s, 3H). ^{13}C NMR (125 MHz, CDCl_3): δ 165.9, 161.3, 157.2, 148.3, 134.6, 129.7, 129.2, 124.3, 115.3, 105.4, 98.8, 55.9, 55.5. HRMS Calcd for $\text{C}_{13}\text{H}_{12}\text{O}_4\text{S}$: $(\text{M} - \text{H})^+$ 263.0378. Found: 263.0376.

5-(2,5-Dimethoxyphenyl)thiophene-2-carboxylic Acid 7{2,18}. Purity: 99%. ^1H NMR (400 MHz, CDCl_3): δ 7.84 (d, $J_{\text{HH}} = 4.0$ Hz, 1H), 7.49 (d, $J_{\text{HH}} = 4.0$ Hz, 1H), 7.24 (br

s, 1H), 6.95–6.87 (m, 2H), 3.92 (s, 3H), 3.82 (s, 3H). ¹³C NMR (125 MHz, CDCl₃): δ 167.3, 153.6, 150.4, 147.6, 134.5, 129.1, 125.7, 122.7, 115.0, 113.6, 113.0, 56.2, 55.9. HRMS Calcd for C₁₃H₁₂O₄S: (M – H)⁺ 263.0378. Found: 263.0375.

Acknowledgment. This investigation was generously supported by partial funds provided by the University of Kansas Research Development Fund, NIH COBRE award (P20 RR015563) with additional funds from the State of Kansas, the National Institutes of General Medical Sciences (KU Chemical Methodologies and Library Development Center of Excellence, P50 GM069663), NIGMS Pilot Scale Libraries Program (NIH P41GM076302-01), and NIH grants R01 AI065898 and P20 RR015563. In addition, the authors would like to thank the NIH K-INBRE program for undergraduate funding (J.G.) and the University of Kansas Honors Program for providing a University of Kansas Undergraduate Research Award (P.G.).

Supporting Information Available. Characterization data for library members including HPLC/MS chromatograms, ¹H and ¹³C NMR for library members, and Lipinski/ADME property table. This material is available free of charge via the Internet at <http://acs.pubs.org/>.

References and Notes

- Bradshaw, R. A.; Brickey, W. W.; Walker, K. W. *Trends Biochem. Sci.* **1998**, *23*, 263–267.
- Chen, S.; Vetro, J. A.; Chang, Y.-H. *Arch. Biochem. Biophys.* **2002**, *398*, 87–93.
- (a) Griffith, E. C.; Su, Z.; Niwayama, S.; Ramsay, C. A.; Chang, Y.-H.; Liu, J. O. *Proc. Natl. Acad. Sci. U.S.A.* **1998**, *95*, 15183–15188. (b) Griffith, E. C.; Su, Z.; Turk, B. E.; Chen, S.; Chang, Y.-H.; Wu, Z.; Biemann, K.; Liu, J. O. *Chem. Biol.* **1997**, *4*, 461–471.
- Towbin, H.; Bair, K. W.; DeCaprio, J. A.; Eck, M. J.; Kim, S.; Kinder, F. R.; Morollo, A.; Mueller, D. R.; Schindler, P.; Song, H. K.; van Oostrum, J.; Versace, R. W.; Voshol, H.; Wood, J.; Zabudoff, S.; Phillips, P. E. *J. Biol. Chem.* **2003**, *278*, 52964–52971.
- Chang, S.-Y.; McGary, E. C.; Chang, S. *J. Bacteriol.* **1989**, *171*, 4071–4072.
- Miller, C. G.; Kukral, A. M.; Miller, J. L.; Movva, N. R. *J. Bacteriol.* **1989**, *171*, 5215–5217.
- Vaughan, M. D.; Sampson, P. B.; Honek, J. F. *Curr. Med. Chem.* **2002**, *9*, 385–409.
- Steinmeyer, A. *ChemMedChem.* **2006**, *1*, 31–36.
- Ye, Q.-Z.; Xie, S.-X.; Huang, M.; Huang, W.-J.; Lu, J.-P.; Ma, Z.-Q. *J. Am. Chem. Soc.* **2004**, *126*, 13940–13941.
- Huang, Q.-Q.; Huang, M.; Nan, F. J.; Ye, Q.-Z. *Bioorg. Med. Chem. Lett.* **2005**, *15*, 5386–5391.
- Vedantham, P.; Zhang, M.; Gor, P. J.; Huang, M.; Georg, G. I.; Lushington, G. H.; Mitscher, L. A.; Ye, Q.-Z.; Hanson, P. R. *J. Comb. Chem.* **2008**, *10*, 195–203.
- McComas, W.; Chen, L.; Kim, K. *Tetrahedron Lett.* **2000**, *41*, 3573–3576.
- Vickerstaffe, E.; Warrington, B. H.; Ladlow, M.; Ley, S. L. *Org. Biomol. Chem.* **2003**, *1*, 2419–2422.
- Jönsson, D.; Warrington, B. H.; Ladlow, M. *J. Comb. Chem.* **2004**, *6*, 584–595.
- Dondoni, A.; Marra, A.; Massi, A. *Angew. Chem., Int. Ed.* **2005**, *44*, 1672–1676.
- (a) Baxendale, I. R.; Ley, S. L.; Martinelli, M. *Tetrahedron* **2005**, *61*, 5323–5349. (b) Adams, G. L.; Graybill, T. L.; Sanchez, R. M.; Maggaard, V. W.; Burton, G.; Rivero, R. A. *Tetrahedron Lett.* **2003**, *44*, 5041–5045.
- Different procedures to improve the yield of the catch–release sequence including capturing the free acid on the resin twice in succession before cleavage and treating the intermediate ion-pair with a higher strength of HCl (4N, 6N, 5–6N in isopropanol) were attempted.
- It was observed that dilute HCl could not be used with MeOH as a solvent for cleavage, since esterification of the final products were observed. For further details, please see Morwick, T. M. *J. Comb. Chem.* **2006**, *8*, 649–651.
- Despite these high purity levels, all compounds were submitted to preparative HPLC (mass-directed fractionation) to ensure the compounds contained no residual color or Pd.
- (a) D'souza, V. M.; Holz, R. C. *Biochemistry* **1999**, *38*, 11079–11085. (b) Li, J.-Y.; Chen, L.-L.; Cui, Y.-M.; Luo, Q.-L.; Li, J.; Nan, F.-J.; Ye, Q.-Z. *Biochem. Biophys. Res. Commun.* **2003**, *307*, 172–179.
- SYBYL 7.2; The Tripos Associates, Inc.: St. Louis, MO, 2006.
- Clark, M.; Cramer, R. D.; Van Opdenbosch, N. *J. Comput. Chem.* **1989**, *10*, 982–1012.
- Gasteiger, J.; Marsili, M. *Tetrahedron Lett.* **1978**, *34*, 3181–3184.
- Morris, G. M.; Goodsell, D. S.; Huey, R.; Olson, A. *J. Computer-Aided Mol. Design* **1996**, *10*, 293–304.
- (a) Wang, T.; Wade, R. C. *J. Med. Chem.* **2002**, *45*, 4828–4837. (b) Guo, J.; Hurley, M. M.; Wright, J. B.; Lushington, G. H. *J. Med. Chem.* **2004**, *47*, 5492–5500.
- SIMCA-P; Umereics AB; Umea, Sweden, 2001.
- pK_A Calculator Plug-In; ChemAxon, Inc.: Budapest, Hungary, 2005.
- SYBYL 6.9.2; The Tripos Associates: St. Louis, MO, 2004.
- Cruciani, G.; Crivori, P.; Carrupt, P.-A.; Testa, B. *THEOCHEM* **2000**, *503*, 17–30.
- Pearlman, R. S.; Smith, K. M. *Drugs Future* **1998**, *23*, 885.

CC700085C